Supporting Information

Cascade Kinetics of an Artificial Metabolon by Molecular Dynamics and Kinetic Monte Carlo

Yuanchao Liu,[a] *Ivana Matanovic,*[b] *David P. Hickey,*[c] *Shelley D. Minteer,**[,c] *Plamen Atanassov,**[,b] *and Scott Calabrese Barton**[,a]

[a]Department of Chemical Engineering and Materials Science, Michigan State University, East Lansing, Michigan 48824, United States

[b]Department of Chemical and Biological Engineering and Center for Micro-Engineered Materials, University of New Mexico, New Mexico 87131, United States

[c]Department of Chemistry, University of Utah, Salt Lake City, Utah 84112, United States

* Shelley D. Minteer: minteer@chem.utah.edu.

* Plamen Atanassov: plamen@unm.edu.

* Scott Calabrese Barton: scb@msu.edu.

Contents

Experiment

The data for experimental lag time was taken from our previous publication and details can be found correspondingly.[1]

Normal MD Simulation

GROMACS 2016.2[2–8] was used as the simulation package. The whole simulation was governed by CHARMM36[9,10] as the force field with CGenFF (CHARMM General Force Field)[11] for the topology of non-standard intermediate molecules. Periodic boundary conditions (PBC) were applied to all MD simulations. The biomolecules were first solvated with tip3p water molecules in a dodecahedral box and then neutralized by explicit Na^+ or Cl^- ions. After that, system energy was minimized using a steepest descent algorithm, and then NVT (0.1 ns) and NPT (1.0 ns) equilibration processes were conducted with position restraints. Finally, a regular MD simulation was performed under NPT ensembles. Unless specified, the system temperature was coupled at 310 K by Velocity-rescale thermostat[12] and the pressure was stabilized at 1 bar by Parrinello-Rahman barostat.[13] Long range electrostatic interaction was calculated by Particle-Mesh Ewald (PME) algorithm with cubic interpolation (0.16 nm grid space).[14,15] Cutoff values for short-range electrostatic and van der Waals interactions were set at 1.2 nm, according to the force field requirement. A Verlet cutoff scheme[16] was used to calculate non-bonded interactions on a GPU accelerator.[17]

Transition state study of hopping energy barrier

The glucose 6 phosphate's (G6P's) hopping rate (k_{hop}) on peptide surface was calculated by the short-range coulombic energy change between the levels of dual- (-400 kJ/mol) and single- (-

200 kJ/mol) association configuration, as shown in Figure 1b.[1] From Transition State Theory (TST) the rate constant, k, is related to the energy barrier ΔG by an Arrhenius expression:

$$k = A \cdot \exp\left(-\frac{\Delta G}{RT}\right) \quad (1)$$

where A is the frequency factor, R is the gas constant and T is the absolute temperature. Therefore, A and ΔG were calculated by fitting ln k versus $1/T$ (Figure 1c). In order to do this, the system was set at 10 temperatures (10, 15, 20, 25, 30, 37, 40, 45, 50, 55 ^{o}C). At each temperature, 10 parallel 100-ns simulations were conducted to calculate the average hopping rate, $k_{hop,}$ and its standard deviation. It should be noted that ΔG and A values were calculated by fitting all of the 10×10 data points. For the ionic strength (IS) dependence study, IS values were set at 0, 20, 40, 70, and 120 mM explicitly represented by Na^+ and Cl^- ions. The IS value here represents additional ion concentration beyond that required for neutralization.

Umbrella Sampling

A dual association configuration was extracted from the MD trajectory of TST study (Figure 2a). After that, the peptide was first restrained at a reference position and the readily adsorbed intermediate molecules (G6P) were pulled away perpendicularly from the peptide for 200 ns, with a spring constant of 1000 kJ mol^{-1} and a pulling rate of 0.01 nm ps^{-1} (Figure 2a). The two corresponding ε-ammonium nitrogen atoms were selected as the reference group and the whole G6P molecule was selected as the pull group. As a result, a maximum distance at 2 nm was achieved for the center-of-mass (COM) of G6P as a reference to its original position. From pulling trajectories, 15 frames with a COM increment of 0.1 nm were selected as the initial configuration for each window in umbrella sampling. Such spacing distance allow sufficient

overlap between the probability distribution within neighboring windows. Finally, 15 ns MD was conducted in each window by umbrella sampling, with two reaction coordinates. Specifically, GROMACS 'COM-distance' and 'COM-direction' modules were used to restrain the G6P's COM around a specific region above peptide surface, with a spring constant of 500 kJ mol^{-1} for each.

In order to calculate the potential of mean force (PMF)[18] as an indication of sorption energy, the sampling results were combined by weighted histogram analysis method (WHAM)[19,20] using Grossfield-WHAM code[21]. As shown in Figure S1, a 2-D PMF with non-independent reaction coordinates was obtained, where x_1 was above mentioned GROMACS 'COM-distance' and x_2 was 'COM-direction'. In other words, x_2 is the projection of x_1 on the vector of initial pulling direction. Then, the 1-D energy profile was obtained by taking the PMF average over x_2 (COM direction) at each x_1 points (COM-distance). The ragged edge of the 2D PMF (Figure S1, left) is due to the insufficient sampling when x1 and x2 were too far away from their energy minimum. Therefore, this region was dropped when calculating the 1-D PMF along x_1. As shown in the figure, the average on x_2 was performed only in the area above the yellow line, where $x_1 - x_2 \leq 0.1$ nm. For IS dependence study, the above simulations were performed at 0, 20, 40, 70, and 120 mM.

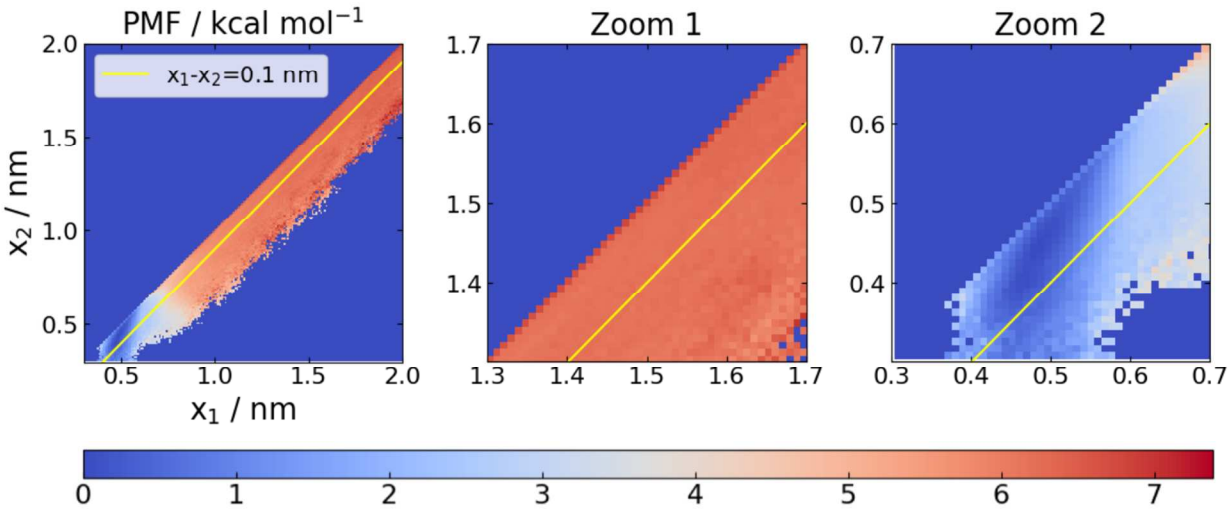

Figure S1. 2D PMF calculated by Grossfield WHAM code.

The probability distributions of x_1 in Figure S1 is shown in Figure S2a, indicating a sufficient overlap between neighboring windows, allowing an effective combination of each relative energy profiles as shown in Figure 2b.

Figure S2b and c show the convergence of PMF profiles with increasing sampling time from 2 ns to 20 ns. Due to the less impact from the bulk ionic environment, the region with low IS and surface distance converged faster. Collectively, the PMF profile converge well after 15 ns. As mentioned above, the PMF with 15 ns sampling time for each window was applied to Figure 2b in the main text. Errors were estimated from the convergence of PMF profiles, by taking the standard deviation of the PMF values at 10-15 ns as shown in Figure S2.

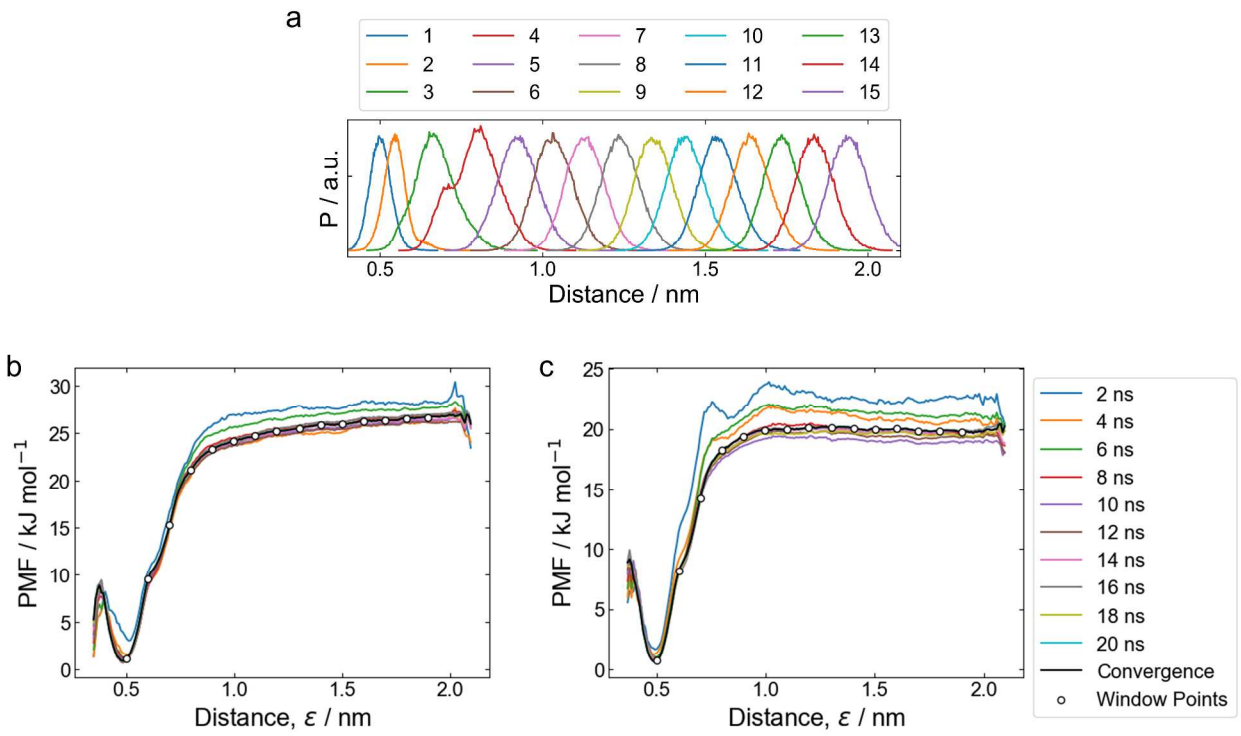

Figure S2. (a) Biased probability distribution of G6P molecule in each window. The reaction coordinate correspond to Figure 1b and the x_1 in Figure S1. Convergence of PMF profile at 0 mM (b) and 120 mM (c) with increasing sampling time from 2ns to 20 ns.

Crystal Structure Selection

In order to have a reasonable enzyme crystal structure, a comparison was made between the experimental G6PDH (*Saccharomyces cerevisiae*)[1] and the G6PDHs with available crystal structure (**Table S1**). According to the charge similarity, Ma_G6PDH and Lm_G6PDH was ruled out. With secondary cofactor binding site, the human G6PDH structure is very different from yeast G6PDH. Moreover, Tc_G6PDH has multiple CYS linker sites and available complex structure with both substrate and cofactor readily adsorbed. Therefore, Tc_G6PDH was selected to study the hopping from LYS bridge to downstream enzyme active site. CYS-528 was selected as the linker site, as it was fully solvent exposed and closed to the G6P binding site.

Table S1. Comparison of experimental G6PDH[1] and available crystal structures.

Enzyme	Sc_G6PDH	Hs_G6PDH	Tc_G6PDH	Ma_G6PDH	Lm_G6PD
Organism	Saccharomyces cerevisiae	Homo sapiens	Trypanosoma Cruzi	Mycobacterium Avium	Leuconostoc Mesenteroides
Species	Eukaryote yeast	Eukaryote human	Eukaryote parasite	Prokaryote bacteria	Prokaryote bacteria
Similarity[a]	--	48%	49%	34%	35%
Similarity + [b]	--	64%	64%	53%	54%
Total charge	-4.6	-1.1	1.1	-18	-21
PDB index	none	2BH9	5AQ1	4LGV	1E7Y
Ligands[c]	--	NADP/G6P	NADP&G6P	no	NADP&G6P
CYS number	single	multi	multi	single	no
CYS proximity[d]	good	medium	very good	medium	--

[a]Similarity: residue similarity to Sc_G6PDH; [b]Similarity +: positive similarity to Sc_G6PDH; [c]Ligands: substrate and cofactor availability in crystal structure; [d]CYS proximity: the proximity of CYS residue to G6P binding site.

Topology hybridization at linker site

The topology of the chemical bond between non-standard BM-$(PEG)_2$ linker molecules[1] and standard CYS residue on G6PDH is acquired by the combination of CHARMM and CGenFF. As shown in Figure S3, the linker molecule was capped with CYS residues on each side using *ChemAxon Marvin Sketch*. Then, the topology of whole complex was generated by CGenFF. The interface topology (bonds, angels, dihedrals) was used for the entire complex in MD simulation (Figure 3b). The independent standard and non-standard sections were still represented by CHARMM and CGenFF, respectively.

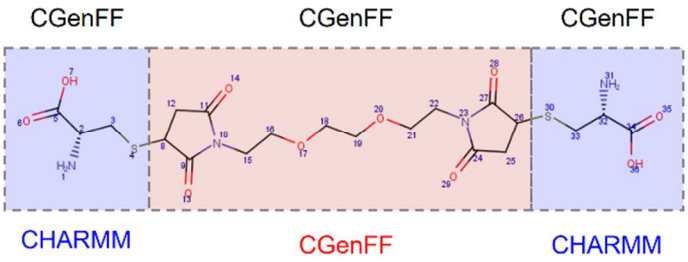

Figure S3. Chemical structure of linker molecule bonded with CYS residue on each side, CYS-(BM-$(PEG)_2$)-CYS.

To stabilize the complex, the terminal HK CYS of the bridge was first pulled away from the position-restrained G6PDH, extending the LYS bridge. Subsequently, the HK CYS side was position restrained while the rest of complex was allowed to stabilize over a 100 ns MD simulation. The resulting complex was used to initialize probability analysis, as shown in Figure 3b.

Transport Probability between Peptide Bridge and Enzyme Active Site.

Using molecular docking, several favorable binding sites of G6P to G6PDH were identified between LYS bridge and the G6P binding pocket (Figure S4). The docking simulations were performed using AutoDock Vina.[22,23] Docking of G6P to G6PDH in the presence of the LYS bridge was performed multiple times using a range of areas (search box sizes) between LYS bridge and the G6PDH active site. As a result, the rest of the area between the bridge and the active site was considered as a potential transition state area, where the position of G6P can be adjusted to find the points as shown in Figure 3a and b.

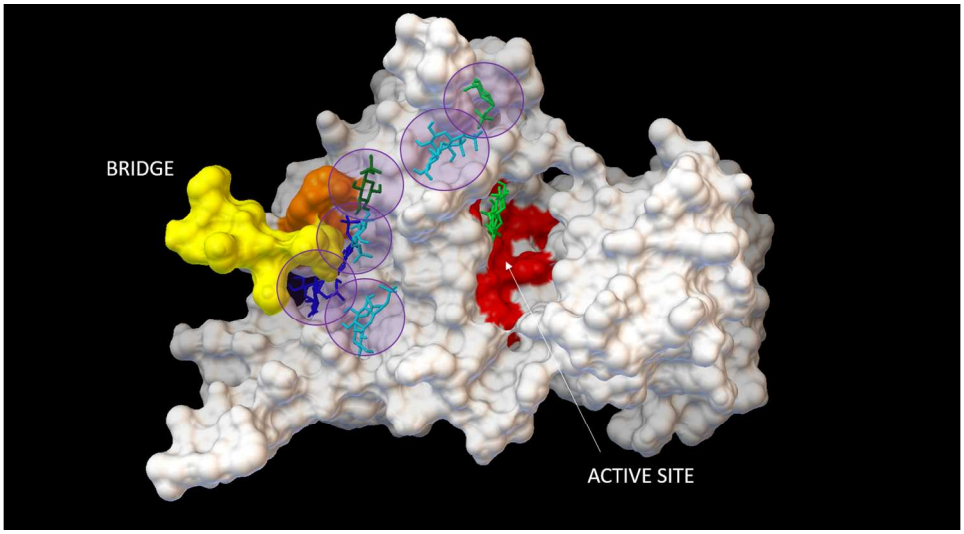

Figure S4. The results of molecular docking simulations for the binding of G6P to G6PDH (circled positions) in the area between LYS bridge and G6P binding pocket on G6PDH.

Using the configuration from Figure 3b as the initial frame, the velocity of all atoms was regenerated and then equilibrated for 1 ns (position restraint on all G6P and complex atoms). After that, 1000 parallel MD simulations (2 ns) were conducted with position restraint only on the HK CYS residue. Based on this, the probability was calculated for three outcomes for the G6P molecule: reaching the peptide bridge (p_{br}), reaching the G6PDH pocket (p_{poc}) or desorbing into the bulk (p_{des}). Each outcome was determined the distance of the G6P center of mass to the corresponding residues. That is, when G6P was within 1.2 nm (short range cut-off) to the LYS bridge surface or the G6P binding pocket, it was assumed to reach the destination. If G6P molecule was 1.2 nm away from the whole complex, it was assumed to desorb. Cases where G6P was located elsewhere on the complex surface after 2 ns (~20% of all simulations) were considered incomplete channeling, and were not included in the calculation. Finally, the initial position of G6P was slightly adjusted until p_{br} is comparable to p_{poc}. Figure S5 shows that the probability became fairly consistent when the simulation was repeated more than 200 times.

Therefore, all the probability results in the main text were calculated from 500 parallel simulations.

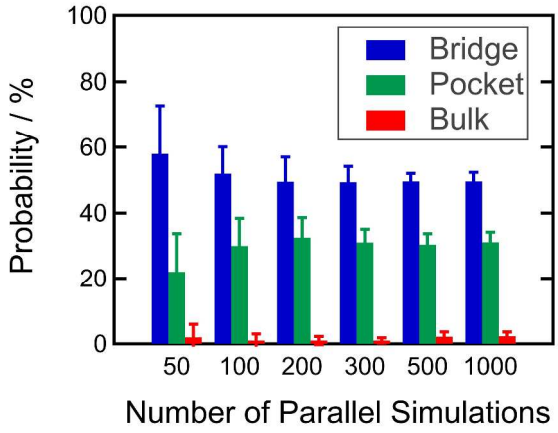

Figure S5. Probability results as a function of number of parallel simulation.

The energy difference between transition state and desorption level was calculated from the resulted probability according to Figure 3a and equation:

$$\Delta G^{\mathrm{BrE2}} = -RT \ln\left(\frac{p_{\mathrm{hop}}^{\mathrm{BrE2}}}{p_{\mathrm{des}}^{\mathrm{BrE2}}}\right) \tag{2}$$

Table S2 summarize all energy values, key rate constant ratios and key probability ratios. With the ΔG^{BrE2} value from probability analysis and assuming a uniform bulk energy level (equation 3), the hopping energy barrier from bridge to G6PDH can be calculated as equation (4).

$$G_{\mathrm{des}}^{\mathrm{BrBr}} = G_{\mathrm{des}}^{\mathrm{BrE2}} \tag{3}$$

$$G_{\mathrm{hop}}^{\mathrm{BrE2}} = G_{\mathrm{des}}^{\mathrm{BrBr}} - \Delta G^{\mathrm{BrE2}} \tag{4}$$

So far, all energy terms were mapped from LYS bridge to G6PDH binding pocket, as shown in **Table S2**.

Table S2. Energy barriers, related rate constants and cascade kinetics.

		Bridge					Bridge to G6PDH		
IS mM	$\boldsymbol{\lambda_{debye}}$ nm	$\boldsymbol{G_{hop}^{BrBr}}$ kJ/mol	$\boldsymbol{G_{des}^{BrBr}}$ kJ/mol	$\boldsymbol{\Delta G^{BrBr}}$ kJ/mol	$\boldsymbol{\frac{k_{hop}^{BrBr}}{k_{des}^{BrBr}}}$	$\boldsymbol{\frac{k_{ads}^{BrBr}}{k_{des}^{BrBr}}}$	$\boldsymbol{\frac{p_{hop}^{BrE2}}{p_{des}^{BrE2}}}$	$\boldsymbol{\Delta G^{BrE2}}$ kJ/mol	$\boldsymbol{G_{hop}^{BrE2}}$ kJ/mol
0	9.8	12	26	14	189	$2.0*10^4$	27	8.5	17
20	2.2	12	25	13	146	$1.5*10^4$	14	6.9	18
40	1.6	12	24	12	99	$1.0*10^4$	11	6.1	18
70	1.2	12	22	9.7	43	$4.5*10^3$	7.4	5.2	17
120	0.9	12	19	7.1	16	$1.7*10^3$	3.3	3.1	16

IS: ionic strength

λ_{debye}: debye length

G_{hop}^{BrBr}, k_{hop}^{BrBr}: energy barrier and rate constant for hopping from one dual association site to neighboring site on LYS bridge

G_{des}^{BrBr}, k_{des}^{BrBr}: energy barrier and rate constant for desorption from one dual association site

k_{ads}^{BrBr}: rate constant for bulk intermediate to adsorb onto one dual association site

ΔG^{BrBr}=G_{des}^{BrBr}-G_{hop}^{BrBr}: energy difference from hopping transition state level to desorption level

p_{des}^{BrE2}: desorption probability for hopping from last dual association site to G6P binding pocket on G6PDH

ΔG^{BrE2}: energy difference between transition state level and desorption level, when hopping from last dual association site to G6P binding pocket on G6PDH

p_{hop}^{BrE2}, ΔG^{BrE2}: probability and energy barrier for hopping from last dual association site to G6P binding pocket on G6PDH

KMC Model

By using Python, kinetic Monte Carlo simulation was conducted. Figure 4a shows the cascade model for KMC simulation, where the two active sites (E_1 and E_2) were connected by several discrete hopping sites. On each site, rate constants (e.g., $k_{\mathrm{hop}}^{\mathrm{left}}$, $k_{\mathrm{hop}}^{\mathrm{right}}$, k_{des}, k_{ads} , k_{cat}) were assigned explicitly to all possible events depending on the nature of the site. All sites were allowed to exchange intermediate with the bulk environment. Given the fast diffusion rate of

G6P (~10^{-5} cm^2 s^{-1}) as compared to the turnover frequency (TOF) of active site (~0.01-0.1 s^{-1}), once the G6P left the cascade surface it was assumed to diffuse immediately into a homogeneous bulk media. Therefore, the bulk environment was only represented by a changing value of intermediate concentration. Hopping was assumed to reversible between bridge sites, but was irreversible from E1 to bridge and bridge to E2. If an event was disallowed, the corresponding k value was set to zero. Figure 4a shows all events allowed events on each site. The actual rates in each KMC step were calculated by taking the product of rate constant and the occupancy (1 or 0) of each site. When calculating the adsorption rate, the bulk concentration will also be added to this product.

Having assigned all rate values (k_1, k_2…k_n) to all available sites, a random number (ρ_1) was generated between 0 and 1, to pick a specific event as shown in equation:

$$\sum_{i=1}^{i_0-1} k_i < \rho_1 \cdot \Gamma_{\text{total}} \leq \sum_{i=1}^{i_0} k_i \tag{5}$$

where Γ_{total} is the summation of all k values in current KMC step. The corresponding event i_0 was then executed and the time evolution, Δt, is calculated by equation:

$$\Delta t = -\ln(\rho_2)/\Gamma_{\text{total}} \tag{6}$$

where ρ_2 is another random number. After event execution, the occupancy and rate values were updated accordingly. Then, KMC simulation entered a loop until the time reached 1000 ns (steady state product evolution from E2). From the time course of product evolution, lag time, τ, was calculated by extrapolating the 500-1000s segment back to the time axis, as shown in Figure 4b.

In each KMC simulation, 100 parallel cascades were employed to enhance the event sampling and reduce the uncertainty of intermediate concentration. Normally, each KMC simulation took less than 10^7 steps, depending the parameters of KMC simulation. Finally, 5 parallel KMC simulations were conducted to evaluate the error of the lag time.

KMC Parameters

Table S3 shows the parameters for KMC simulation. Specifically, TOFs on E1 ($k_{\mathrm{cat}}^{\mathrm{E1}}$) and E2 ($k_{\mathrm{cat}}^{\mathrm{E2}}$) was calculated by fitting the steady state product evolution of a fully saturated HK and G6PDH in experiment.[1] On each active site, substrate desorption rate constant, k_{des}, was taken as 1/10 of the TOF, in order to minimize the leakage of a readily channeled intermediate. Michaelis constant for E2, K_{M}, was calculated from the experiment lag time of a free-standing system, τ_{free}, at 120 mM according to equation:

$$k_{\mathrm{cat}}^{\mathrm{E1}} = k_{\mathrm{cat}}^{\mathrm{E2}} \times \frac{[I]}{K_{\mathrm{M},2} + [I]} = k_{\mathrm{cat}}^{\mathrm{E2}} \times \frac{k_{\mathrm{cat}}^{\mathrm{E1}} \cdot \tau_{\mathrm{free}}}{K_{\mathrm{M},2} + k_{\mathrm{cat}}^{\mathrm{E1}} \cdot \tau_{\mathrm{free}}} \tag{7}$$

where [I] is the intermediate concentration at steady state. The $K_{\mathrm{M},2}$ at other IS environment was assumed to be identical, in order to avoid introducing too may uncertain parameters into the KMC model. Based on this, the channeling efficiency was evaluated by incorporating the channeling parameters from MD simulations.

The adsorption rate constants, $k_{\mathrm{ads}}^{\mathrm{E2}}$, were calculated according to following equation:

$$k_{\mathrm{ads}}^{\mathrm{E2}} = \frac{k_{\mathrm{cat}}^{\mathrm{E2}} + k_{\mathrm{des}}^{\mathrm{E2}}}{K_{\mathrm{M},2}} \tag{8}$$

Then, system volume, *vol*, was calculated based the cascade concentration and number of parallel cascades. As a result, the concentration of leakage and hop (Figure 5b and c) was

calculated from the explicit event numbers, Avogadro number and volume. In this way, the degree of leakage and hop could be compared directly with product and intermediate evolution. Substrate concentration for E1 was 2 mol/L, making E1 fully saturated through the entire KMC time scale considering the consumption of substrate molecules.

Besides the above-mentioned experimentally determined parameters, the rate constants for bridge-E2 channeling were obtained from MD results, as shown in **Table S2**. The hopping rate (~ ns^{-1}) on the peptide bridge is orders of magnitude higher than the TOF on each active site (~ s-1), such that enzyme turnover is rate limiting. Therefore, equilibrium ratios of respective rates govern the channeling process. In actual KMC simulation, k_{hop} was set at two orders of magnitude higher than $k_{\mathrm{cat}}^{\mathrm{E1}}$, to improve simulation efficiency. Meanwhile, ratios of k_{hop}, k_{des}, k_{ads} and $k_{\mathrm{hop}}^{\mathrm{b2}}$ were consistent with the MD simulation results (**Table S2**). This guarantees the leaking probability for each individual KMC event is the same as the dynamic behavior observed in MD. For the IS dependent study, the rate values were calculated according to the rate constant ratios in **Table S2**.

Table S3. KMC parameters.

Constant	Value
c_{E1E2}, cascade concentration / mol/L	$8*10^{-9}$
vol, compartment volume / L	$2.1*10^{-14}$
c_{sub}, concentration of substrate for E1 / mol/L	2
$k_{\mathrm{cat}}^{\mathrm{E1}}$, TOF on E1 / molec s^{-1}	0.7
$k_{\mathrm{des}}^{\mathrm{E1}}$, desorption rate on E1, s^{-1}	0.07
$k_{\mathrm{ads}}^{\mathrm{E1}}$, adsorption rate on E1, s^{-1} M^{-1}	$7.7*10^{5}$
$k_{\mathrm{hop}}^{\mathrm{1b}}$, hopping rate from E1 to bridge, s^{-1}	$7*10^{15}$
$K_{\mathrm{M,1}}$, Michaelis Constant of E1, mM	10^{-2}
$k_{\mathrm{cat}}^{\mathrm{E2}}$, TOF on E2 / molec s^{-1}	6.2
$k_{\mathrm{des}}^{\mathrm{E2}}$, desorption rate on E2, s^{-1}	0.62
$k_{\mathrm{ads}}^{\mathrm{E2}}$, adsorption rate on E2, s^{-1} M^{-1}	$1.3*10^{6}$
$K_{\mathrm{M,2}}$, Michaelis Constant of E2, mM	$5.4*10^{-3}$
k_{hop}, hopping rate on bridge, s^{-1}	$k_{\mathrm{cat}}^{\mathrm{E1}} \times 100$
k_{des}, desorption rate on bridge, s^{-1}	$k_{\mathrm{hop}} \,/\, (189, 146, 99, 43, 16)$
k_{ads}, adsorption rate on bridge, s^{-1} mol^{-1} L	$k_{des} \times (20, 15, 10, 4.5, 1.7) \times 10^{3}$
$k_{\mathrm{hop}}^{\mathrm{b2}}$, hopping rate from bridge to E2, s^{-1}	$k_{\mathrm{des}} \times (27, 14, 11, 7.4, 3.3)$

REFERENCES

(1) Liu, Y.; Hickey, D. P.; Guo, J.-Y.; Earl, E.; Abdellaoui, S.; Milton, R. D.; Sigman, M. S.; Minteer, S. D.; Calabrese Barton, S. Substrate Channeling in an Artificial Metabolon: A Molecular Dynamics Blueprint for an Experimental Peptide Bridge. *ACS Catal.* **2017**, *7*, 2486–2493.

(2) Berendsen, H. J. C.; van der Spoel, D.; van Drunen, R. GROMACS: A Message-Passing Parallel Molecular Dynamics Implementation. *Comput. Phys. Commun.* **1995**, *91*, 43–56.

(3) Lindahl, E.; Hess, B.; van der Spoel, D. GROMACS 3.0: A Package for Molecular Simulation and Trajectory Analysis. *J. Mol. Model.* **2001**, *7*, 306–317.

(4) Hess, B.; Kutzner, C.; van der Spoel, D.; Lindahl, E. GROMACS 4: Algorithms for Highly Efficient, Load-Balanced, and Scalable Molecular Simulation. *J. Chem. Theory Comput.* **2008**, *4*, 435–447.

(5) Pronk, S.; Pall, S.; Schulz, R.; Larsson, P.; Bjelkmar, P.; Apostolov, R.; Shirts, M. R.; Smith, J. C.; Kasson, P. M.; van der Spoel, D.; Hess, B.; Lindahl, E. GROMACS 4.5: A High-Throughput and Highly Parallel Open Source Molecular Simulation Toolkit. *Bioinformatics* **2013**, *29*, 845–854.

(6) Abraham, M. J.; Murtola, T.; Schulz, R.; Páll, S.; Smith, J. C.; Hess, B.; Lindahl, E. GROMACS: High Performance Molecular Simulations through Multi-Level Parallelism from Laptops to Supercomputers. *SoftwareX* **2015**, *1–2*, 19–25.

(7) Van Der Spoel, D.; Lindahl, E.; Hess, B.; Groenhof, G.; Mark, A. E.; Berendsen, H. J. C. GROMACS: Fast, Flexible, and Free. *J. Comput. Chem.* **2005**, *26*, 1701–1718.

(8) Páll, S.; Abraham, M. J.; Kutzner, C.; Hess, B.; Lindahl, E. Tackling Exascale Software Challenges in Molecular Dynamics Simulations with GROMACS. In *Solving Software Challenges for Exascale*; Markidis, S., Laure, E., Eds.; Springer International Publishing: Cham (Switzerland), 2015; pp 3–27.

(9) Brooks, B. R.; Bruccoleri, R. E.; Olafson, B. D.; States, D. J.; Swaminathan, S.; Karplus, M. CHARMM: A Program for Macromolecular Energy, Minimization, and Dynamics Calculations. *J. Comput. Chem.* **1983**, *4*, 187–217.

(10) Best, R. B.; Zhu, X.; Shim, J.; Lopes, P. E. M.; Mittal, J.; Feig, M.; MacKerell, A. D. Optimization of the Additive CHARMM All-Atom Protein Force Field Targeting Improved Sampling of the Backbone ϕ, ψ and Side-Chain χ 1 and χ 2 Dihedral Angles. *J. Chem. Theory Comput.* **2012**, *8*, 3257–3273.

(11) Vanommeslaeghe, K.; Hatcher, E.; Acharya, C.; Kundu, S.; Zhong, S.; Shim, J.; Darian, E.; Guvench, O.; Lopes, P.; Vorobyov, I.; Mackerell, A. D. CHARMM General Force Field: A Force Field for Drug-like Molecules Compatible with the CHARMM All-Atom Additive Biological Force Fields. *J. Comput. Chem.* **2009**, *31*, 471–690.

(12) Bussi, G.; Donadio, D.; Parrinello, M. Canonical Sampling through Velocity Rescaling. *J. Chem. Phys.* **2007**, *126*, 014101.

(13) Parrinello, M.; Rahman, A. Polymorphic Transitions in Single Crystals: A New Molecular Dynamics Method. *J. Appl. Phys.* **1981**, *52*, 7182–7190.

(14) Wennberg, C. L.; Murtola, T.; Hess, B.; Lindahl, E. Lennard-Jones Lattice Summation in Bilayer Simulations Has Critical Effects on Surface Tension and Lipid Properties. *J. Chem. Theory Comput.* **2013**, *9*, 3527–3537.

(15) Wennberg, C. L.; Murtola, T.; Páll, S.; Abraham, M. J.; Hess, B.; Lindahl, E. Direct-Space Corrections Enable Fast and Accurate Lorentz–Berthelot Combination Rule Lennard-Jones Lattice Summation. *J. Chem. Theory Comput.* **2015**, *11*, 5737–5746.

(16) Páll, S.; Hess, B. A Flexible Algorithm for Calculating Pair Interactions on SIMD Architectures. *Comput. Phys. Commun.* **2013**, *184*, 2641–2650.

(17) Kutzner, C.; Páll, S.; Fechner, M.; Esztermann, A.; de Groot, B. L.; Grubmüller, H. Best Bang for Your Buck: GPU Nodes for GROMACS Biomolecular Simulations. *J. Comput. Chem.* **2015**, *36*, 1990–2008.

(18) Roux, B. The Calculation of the Potential of Mean Force Using Computer Simulations. *Comput. Phys. Commun.* **1995**, *91*, 275–282.

(19) Souaille, M.; Roux, B. Extension to the Weighted Histogram Analysis Method: Combining Umbrella Sampling with Free Energy Calculations. *Comput. Phys. Commun.* **2001**, *135*, 40–57.

(20) Kumar, S.; Rosenberg, J. M.; Bouzida, D.; Swendsen, R. H.; Kollman, P. A. THE Weighted Histogram Analysis Method for Free-Energy Calculations on Biomolecules. I. The Method. *J. Comput. Chem.* **1992**, *13*, 1011–1021.

(21) Grossfield, A. WHAM: the weighted histogram analysis method. Version 2.0.9 http://membrane.urmc.rochester.edu/content/wham (accessed Aug 17, 2017).

(22) Trott, O.; Olson, A. J. AutoDock Vina: Improving the Speed and Accuracy of Docking with a New Scoring Function, Efficient Optimization, and Multithreading. *J. Comput. Chem.* **2009**, *31*, 671–690.

(23) Sanner, M. F. Python: A Programming Language for Software Integration and Development. *J. Mol. Graph. Model.* **1999**, *17*, 57–61.